Electrochimica Acta 322 (2019) 134725

Contents lists available at ScienceDirect

Electrochimica Acta

journal homepage: www.elsevier.com/locate/electacta

Converting glycerol aqueous solution to hydrogen energy and dihydroxyacetone by the $BiVO_4$ photoelectrochemical cell

Lu-Wei Huang [1], Truong-Giang Vo [1], Chia-Ying Chiang*

Department of Chemical Engineering, National Taiwan University of Science and Technology, Taipei, Taiwan

ARTICLE INFO

Article history:
Received 15 October 2018
Received in revised form
11 August 2019
Accepted 18 August 2019
Available online 22 August 2019

Keywords:
$BiVO_4$
Photoelectrochemical glycerol oxidation
Dihydroxyacetone

ABSTRACT

Replacement of oxygen evolution reaction (OER) by the more readily oxidized biomass derivatives is considered to be a promising strategy for photoelectrocatalytic water splitting hydrogen production. In this work, a biodiesel industrial waste by-product, glycerol, played the critical role for the efficient hydrogen production as well as the highly valuable dihydroxyacetone (DHA) and industrial useful formic acid production. As the glycerol was introduced, a remarkable cathodic shift of the onset potential was observed (~300 mV) while the current density was 4 times higher compared to the water oxidation. The incident photon-to-current efficiency (IPCE) of $BiVO_4$ photoanode for glycerol oxidation reached about 55%, which was 3 times higher than the system without glycerol. More importantly, during the photoelectrochemical water splitting in glycerol aqueous solution, in addition to the evolved hydrogen gas, glycerol was oxidized to valuable products with 15% dihydroxyacetone (DHA) and 85% formic acid. This strategy not only boosts the hydrogen production efficiency, keeps the photoanode very stable but also makes the biodiesel production more profitable and sustainable.

1. Introduction

Each year, the glycerol was produced increasingly in Europe, from 2.4 million tonnes in 2012 to 4.3 million tonnes in 2015, far exceeding the world's glycerol needs in industries, i.e. 2 million tonnes/year in 2015 [1–3]. This is mainly due to the highly promoted biodiesel industry. In the biodiesel production process, the by-product, glycerol, consisting of 10 wt% of the products, was generated. However, due to its vast amount and high viscosity property [4,5], the purification cost limits the overall biodiesel production profit. In order to maximize the sustainability of the biodiesel plant as well as considering the environmental protection, the process of converting glycerol into other compounds were proposed [6,7]. Yet, most of the processes would lead to a wide variety of products which increases the difficulty in separation [8]. In order to overcome this issue, using a photoelectrochemical (PEC) cell with the energy mainly provided by the sun while the products can be tuned by selecting the right catalyst material, it can provide a new sustainable pathway to utilize the waste glycerol.

Recent perspective reports carefully lined out the possible pathways to the electrochemical solar-hydrogen technologies and the technoeconomics of valuable chemicals production by using sunlight [9–11], all of these studies indicated that using an PEC cell to convert sunlight for water splitting hydrogen generation, i.e. the most widely studied approach of PEC energy converting tech, suffers serious difficulties such as not efficient enough and low product value comparing to its high cost process. One might open a new route of PEC by integrating the hydrogen generation at cathode and valuable products production at anode to boost the overall economic value [12]. Valuable molecules like Cl_2, Br_2, H_2O_2 have been generated at anode in a PEC cell with much higher efficiency [11] while some biomass-derivatives, like glucose, with lower thermodynamics and kinetics barrier can be oxidized to boost the overall PEC efficiency [13]. Take TiO_2 as an example, in 1972, Fujishima and Honda first realized the idea of converting solar energy into chemical energy by water splitting reaction ($2H_2O \rightarrow 2H_2 + O_2$) with a wide bandgap TiO_2 as the PEC photoanode [14]. Recently, Augualiaro and co-workers found that TiO_2 can convert glycerol into the highly valuable product, dihydroxyacetone (DHA), at the selectivity of 7.2% [15]. It is worth to note that the price for DHA and purified glycerol are ca. 150 USD/kg and 0.6 USD/kg, respectively. This four-orders of magnitude difference in price gained lots of attention. As in previous report, depositing TiO_2 on carbon supported Ni catalyst for glycerol electro-oxidation, the

* Corresponding author.
E-mail address: cychiang@mail.ntust.edu.tw (C.-Y. Chiang).
[1] These authors contributed equally to this work.

https://doi.org/10.1016/j.electacta.2019.134725
0013-4686/

selectivity of DHA was as low as 4% only [16]. In this year, Guo and co-workers discovered that when the Au containing catalyst was deposited on TiO_2, the selectivity of DHA can be promoted to 66% [17]. Among the glycerol oxidation electrocatalyst studies, precious metals like Au and Pt have shown some high selectivity towards DHA [17–24], however, the price of these catalysts limits the possibility in industrial applications. So, in this study, we aim to find a cheaper PEC material that could absorb more sun light, i.e. smaller bandgap material, and has the ability to convert glycerol into DHA at a higher selectivity.

Among the photoanode materials, $BiVO_4$, with a direct bandgap of 2.4 eV [25,26] and the optical penetration depth ca. 100–500 nm at the wavelength of 420–530 nm [27], shows the potential. However, as in the widely studied water splitting reaction, $BiVO_4$ photoanode suffers from the serious charge recombination and the low water oxidation kinetics thus limiting its water splitting efficiency [26,28]. More precisely, the diffusion lengths of electron and hole in $BiVO_4$ are only ~10 nm and 100–200 nm, respectively [29–31]. Combining with the slow kinetics towards water oxidation, the photon-excited electron-hole pairs show a very short lifetime. With the pros and cons of $BiVO_4$ for water splitting reaction in mind, using glycerol oxidation to replace the slow kinetics water oxidation in a PEC cell might show a brand-new story.

In terms of kinetics, usually, the alcohols like methanol, ethanol, and ethylene glycol can be easily oxidized by the photon generated holes as demonstrated in several previous PEC studies based on TiO_2 and Fe_2O_3 photoanodes [32–35]. More importantly, from the perspective of thermodynamics, the alcohol oxidation requires much less energy than water oxidation [22]. Based on this information, in this study, we would demonstrate that the $BiVO_4$ photoanode can work much more efficient in the oxidation of glycerol comparing to the oxidation of water. More importantly, the high selectivity towards DHA by this earth abundant photocatalyst can be achieved while the clean hydrogen energy can be produced at the cathode.

2. Material and method

2.1. Synthesis of $BiVO_4$ photoanode

The $BiVO_4$ photoanode preparation process was carefully addressed in our previous reports [26,36] and would be briefly described here. Two precursors, bismuth nitrate ($Bi(NO_3)_3 \cdot 5H_2O$) and vanadyl acetylacetonate ($VO(acac)_2$), were dissolved in a mixing solvent consisting of 2,4-pentanedione and acetic acid. This solution was filtered by a 0.22 μm nylon filter and spin-coated on a FTO glass substrate at 2500 rpm for 20 s per layer. The effective $BiVO_4$ area was 2 cm × 2 cm. Each spin-coated layer was heated at 500 °C in a muffle furnace. For layer 1–3, layer 4–6 and the last layer, the heating process was last for 10 min, 2 h and 4 h, respectively.

2.2. Characterizations

The surface morphology and thickness of $BiVO_4$ photoanode was studied by a field emission scanning electron microscope (FESEM, JEOL JSM 6500F). High-resolution transmission electron microscopy (HRTEM) was carried out using Tecnai G2 F20 operating at 200 kV. The crystal structure was characterized by X-ray diffraction (Bruker D2 Phaser) with 2θ ranging in 10-70° using Cu Kα radiation. The absorption spectrum of the $BiVO_4$ was measured by the UV–vis spectrophotometer (Jasco V650, Japan). The Raman spectra and mapping image were obtained by Micro Raman system (MRI532S, Protrustech Co., Ltd., Taiwan) using a 532-nm laser as excitation source. X-ray photoelectron spectroscopy (XPS, Thermo Scientific ESCALAB 250) was used for the surface element composition analysis. Inductively coupled plasma atomic emission spectrometry (ICP-AES, JY2000 Jobin Yvon) was performed to determine the chemical composition of the $BiVO_4$ catalysts before and after reaction.

2.3. Photoelectrochemical study and product analysis

The $BiVO_4$ photoelectrochemical (PEC) performance was conducted by an Autolab potentiostat (PGSTAT302N) with a three-electrode configuration. The 2.0 cm × 2.0 cm size samples were used as working electrode while 2.5 cm × 2.5 cm Pt mesh (100 mesh) and an Ag/AgCl (3 M KCl) electrode were employed as a counter and reference electrodes, respectively. The solution used in the PEC study was 0.1 M $Na_2B_4O_7$ (NaBi, pH 9.4) aqueous solution including various glycerol concentrations, i.e. 0, 0.1, 0.5, 1.0, 2.0, and 3.0 M. The photoanode was irradiated by a 500 W solar simulator (Model 66905, Newport) with an AM 1.5 G filter from front-side (semiconductor side). The intensity of the incident light was calibrated to be 1 sun (100 mW/cm^2) by a reference cell with a readout meter (Model 91150V, Newport). For the linear sweep voltammetry (LSV), the scan started from −0.6 V to 0.8 V vs. Ag/AgCl with scan rate of 10 mV/s. Electrochemical impedance spectra (EIS) were obtained in the frequency range of 0.1–10,000 Hz at the set potential of 0.7 V_{RHE}. Incident photon-to-current efficiency (IPCE) was recorded with respect to varying wavelength of incident light (ranging from 350–550 nm) using 500 W xenon arc lamp attached with a monochromator (Oriel Cornerstone 130, Newport).

Gaseous products were analyzed by a gas chromatography (China Chromatography 8900, Taiwan) equipped with a thermal conductivity detector (TCD) and a stainless steel molecular sieve 5A packed column (3 m length). The glycerol oxidation products were quantified by a high-performance liquid chromatographer (HPLC) (Young Lin YL-9100) with an ion-exclusion column (RCM-Monosaccharide Ca^{+2} (8%), Phenomenex). The photodiode array detector was installed for the multiple-wavelength detection simultaneously. The mobile phase was 0.01 M H_3PO_4 aqueous solution with a flow rate of 0.5 mL/min. The column temperature was set at 70 °C.

3. Results and discussion

3.1. $BiVO_4$ photoanode characterization

The film morphology and thickness of the $BiVO_4$ was studied by the scanning electron microscope as shown in Fig. 1. The bird-eye view SEM image highlighted that the $BiVO_4$ layer was densely-packed, while the cross-section image showed the thickness of $BiVO_4$ was about 330 nm. The particle size ranged around 200 nm in diameter. Moreover, the chemical composition of the films was confirmed by X-ray diffraction (XRD) patterns as shown in Fig. 1(c). The diffraction peaks at 2θ of 18.7 and 28.9° corresponded to the scheelite-monoclinic $BiVO_4$ structure (JCPDS 14-0688) while 2θ of 26.6, 33.8, 37.9 and 51.8° came from the FTO substrate (JCPDS 41-1445), indicating that high purity monoclinic $BiVO_4$ was obtained without any other metal oxides or phase segregation. HRTEM analysis was further employed to confirm the monoclinic structure and preferential orientation of $BiVO_4$ thin film. Fig. S1 shows the rim of rounded shape ellipsoidal grains with clear lattice fringes indicating as-prepared $BiVO_4$ possesses well crystalline monoclinic structure. For further information on crystal structure elucidation, Raman spectrum in the 200-1000 cm^{-1} region was presented in Fig. 1(d). The spectrum showed a good agreement with those previous reports for scheelite monoclinic $BiVO_4$ that have typical and distinctive vibrational bands at about 125, 207, 337, 369, and

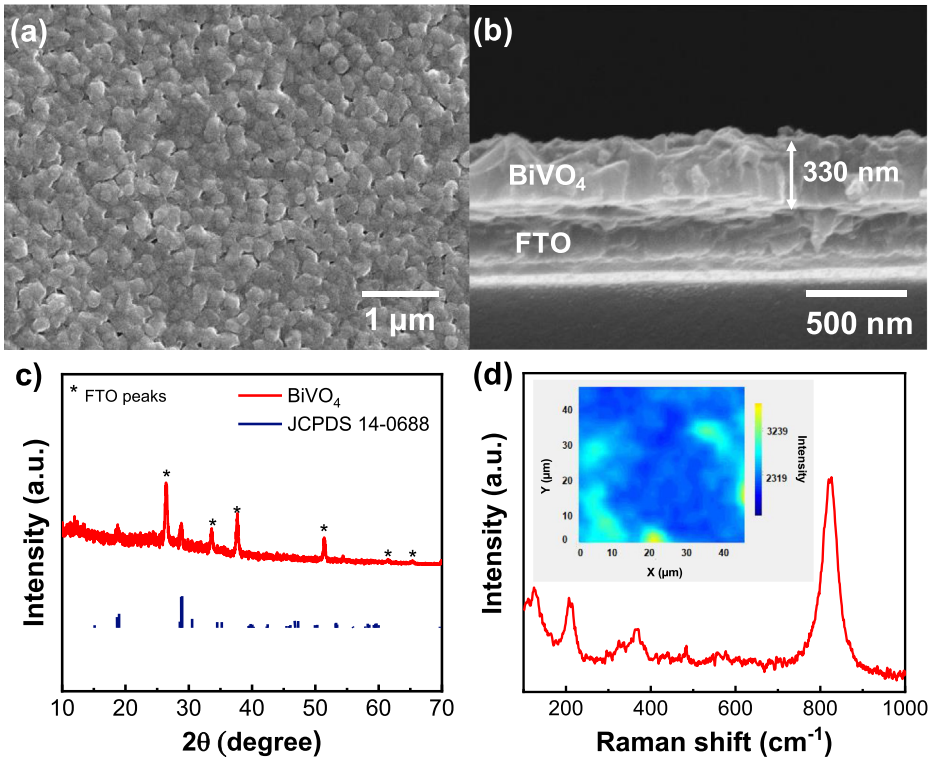

Fig. 1. (a) Top-view and (b) side-view of $BiVO_4$ photoanode; (c) XRD pattern and (d) Raman spectrum of $BiVO_4$. The inset shows Raman mapping image.

826 cm^{-1}. Additionally, the spatial distribution of the crystallized region was explored by performing 2D Raman mapping (inset of Fig. 1(d)). The different in colors represents different Raman signal intensity which implies the different in crystallization degree. As shown in the mapping, $BiVO_4$ exhibited a homogeneous distribution with crystalline $BiVO_4$. This feature is believed to play a critical role in enhancing the catalytic performance of $BiVO_4$ electrode [25].

The light absorbing behavior of the $BiVO_4$ photoanode can be demonstrated by the UV–Vis absorbance spectrum. Based on the absorbance spectrum, the bandgap of $BiVO_4$ can be determined by the Tauc plot, i.e. $(\alpha h\nu)^n$ against photon energy ($h\nu$) where n is an index depending on the nature of optical transition, with value of 2 for direct transition, α is the absorption coefficient, h is the Plank constant, ν is the frequency, and λ is the detection wavelength. As in Fig. 2, the light absorption of $BiVO_4$ started around 510 nm and the bandgap ~2.4 eV can thus be obtained from the x-axis intercept of the linear fit to the Tauc plot (inset) based on Eq. (1), where A is a constant.

$$(\alpha h\nu)^2 = A(h\nu - Eg) \quad (1)$$

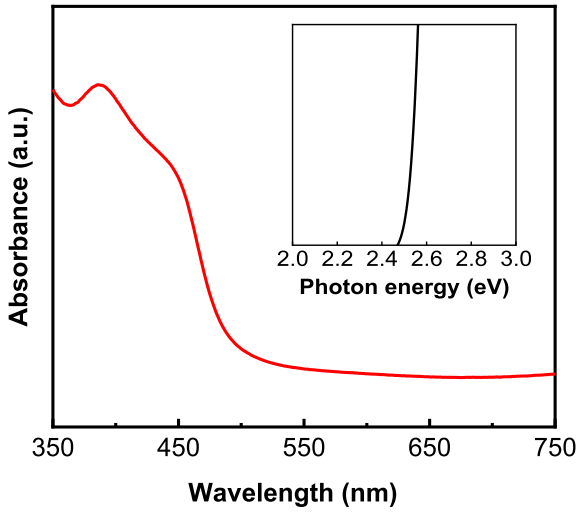

Fig. 2. UV/Vis spectrum and Tauc plot (the inset) of $BiVO_4$ photoanode.

3.2. Photoelectrochemical study

Among the PEC studies, the current density at 1.23 V_{RHE} and the onset potential were two main criteria for the comparison between various $BiVO_4$ PEC efficiencies. As shown in Fig. 3, when there was no light irradiation (dash line), the current density was zero throughout the potential rage of 0.2–1.3 V_{RHE}, and this indicated that a much higher energy would be required to trigger the water oxidation reaction (also named as oxygen evolution reaction, OER) on $BiVO_4$ electrode. Upon the 1 sun AM 1.5 G light irradiation applied, the onset potential and the photocurrent density at 1.23 V_{RHE} of $BiVO_4$ photoanode for OER was around 0.6 V_{RHE} and 0.35 mA/cm^2, respectively. However, as the glycerol was introduced, a clear cathodic shift of the onset potential to ~0.33 V_{RHE} was observed, indicating that the $BiVO_4$ is more favorable in working on the glycerol oxidation. The current density at 1.23 V_{RHE} was almost four times higher comparing to the OER. On the other hand, to reach 0.32 mA/cm^2, with the OER, it needed 1.23 V_{RHE} but only as low as 0.5 V_{RHE} is needed when introducing the glycerol. This clearly indicated that the energy consumption can be highly reduced for an PEC cell when the glycerol was introduced. However, it is not always showing a positive effect when the glycerol concentration increased unlimitedly. As in the figure, as the glycerol

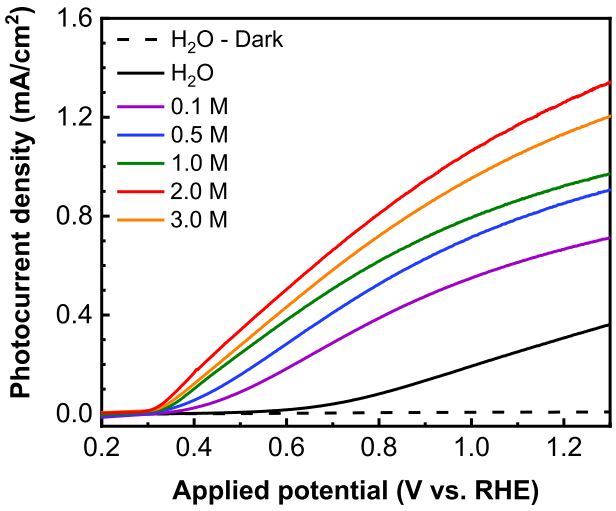

Fig. 3. Current (J)-potential (V) curves of $BiVO_4$ were measured under dark and simulated AM 1.5 G solar light illumination in 0.1 M NaBi electrolyte in presence of various glycerol concentrations (0–3.0 M) with the scanning rate of 10 mV/s.

concentration was relatively low, i.e. 0.1 M–2 M, the current density increased as the concentration increased. This is because that the increasing amount of reactant (glycerol) near the $BiVO_4$ photoanode surface could boost the rate of glycerol oxidation by the photon-excited charge carrier. On the contrary, further increase of the glycerol concentration to 3.0 M hindered this benefit due to the high viscosity of the glycerol, leading to the mass transfer control region where the diffusion took place as the rate determine step. This can be further analyzed by the electrochemical impedance spectroscopy (EIS) study.

As in Fig. 4, the impedance was conducted at 0.7 V_{RHE}, where both OER and glycerol oxidation reaction happened. It is clear that the charge transfer resistance was much higher for OER comparing to the glycerol oxidation reaction and this will be demonstrated later in the charge injection efficiency measurement. With a closer observation, the solution resistance (R_s) increased as the glycerol concentration increased. This is again due to the viscous (low diffusion coefficient) and non-conductive traits of glycerol. The EIS results were further organized into Fig. 4(b), which shows the effects of solution resistance (R_s) and charge transfer resistance (R_{ct}) on the current density. When there was no glycerol added, an extremely high charge transfer resistance but low solution resistance was observed. However, as glycerol was introduced, the R_{ct} dropped apparently while the R_s slowly increased. The change of these two resistances based on the glycerol concentration eventually led to an optimal glycerol concentration (2.0 M) for the most efficient, i.e. highest current density, PEC cell.

In order to demonstrate the ability of glycerol instantly reacting with the photon-generated holes on $BiVO_4$ photoanode, a set of sulfite, known as a hole-sacrificial reagent, oxidation experiment was performed under 1 sun AM 1.5 G irradiation for comparison. The kinetics of sulfite oxidation is considered as extremely fast to allow every hole reaching the electrode-electrolyte interface being oxidized instantly and thus the charge carrier, hole, injection efficiency (η_{inj}) is taken to be 100% [37]. Based on the measured photocurrent density (J_{ph}) of an PEC cell and the relationship of three photocurrent density affecting factors, i.e. the current density converted from the incident light with no energy loss (J_{abs}), the separation efficiency of photon-excited charge carriers (η_{sep}), and the charge injection efficiency (η_{inj}), an equation (Eq. (2)) can be used to express the relationship.

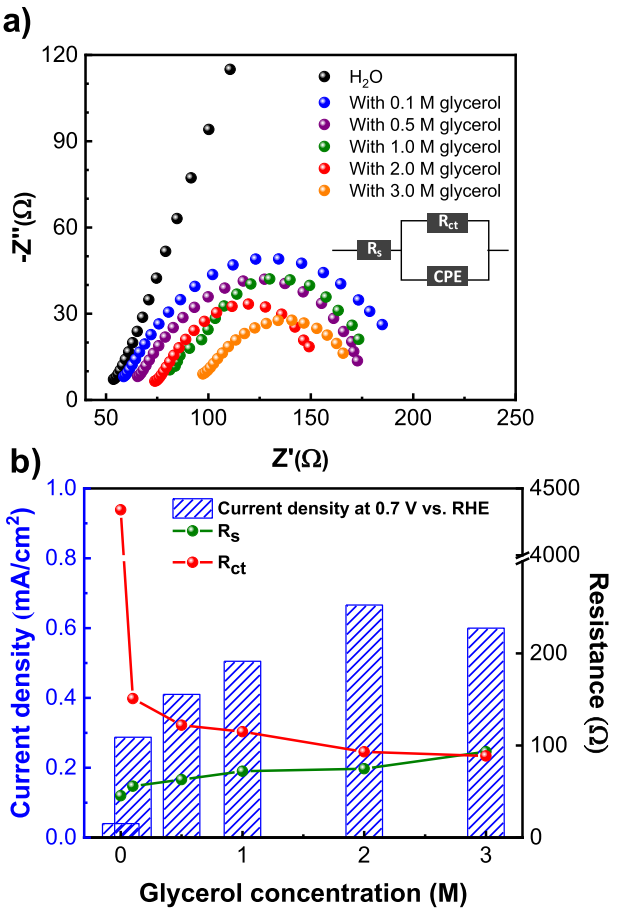

Fig. 4. (a) Nyquist plots of $BiVO_4$ photoanode with different concentration of glycerol at 0.7 V (vs. RHE) under AM 1.5G irradiation; (b) relationship among current density, charge transfer resistance and solution resistance derived from Nyquist plot.

$$J_{ph} = J_{abs} \times \eta_{sep} \times \eta_{inj} \quad (2)$$

With using the same $BiVO_4$ photoanode, the J_{abs} and η_{sep} considered to be the same for water, glycerol and sulfite oxidations. As a result, the difference in the measured current density (J_{ph}) is due to the difference of the hole injection efficiency (η_{inj}). The original LSV of these oxidation reactions was shown in Fig. 5(a). It is clear that the oxidation of water demonstrated relatively low current density as to the sulfite oxidation in all potential range, indicating the low injection efficiency of the hole for water oxidation reaction. However, as 0.1 M glycerol was added, the current density was increased, yet still lower than that of sulfite oxidation. With further increasing the glycerol concentration to 2 M, the surprising result was obtained. The current density was comparable to that of sulfite oxidation, indicating much more charge carrier was generated in the system. It is worth to note that this charge carrier came from the photon excitation as there was no current observed under the dark condition. A further comparison can be made by the ratio of J_{ph} for water and glycerol oxidations (noted as J_{ph}^{rxn}, where rxn represented as water or glycerol oxidation reaction) to sulfite oxidation which led to the hole injection efficiency (η_{inj}) for the water and glycerol oxidations, as shown in Eq. (3) ~ Eq. (5).

$$J_{ph}^{rxn} = J_{abs} \times \eta_{sep} \times \eta_{inj} \quad (3)$$

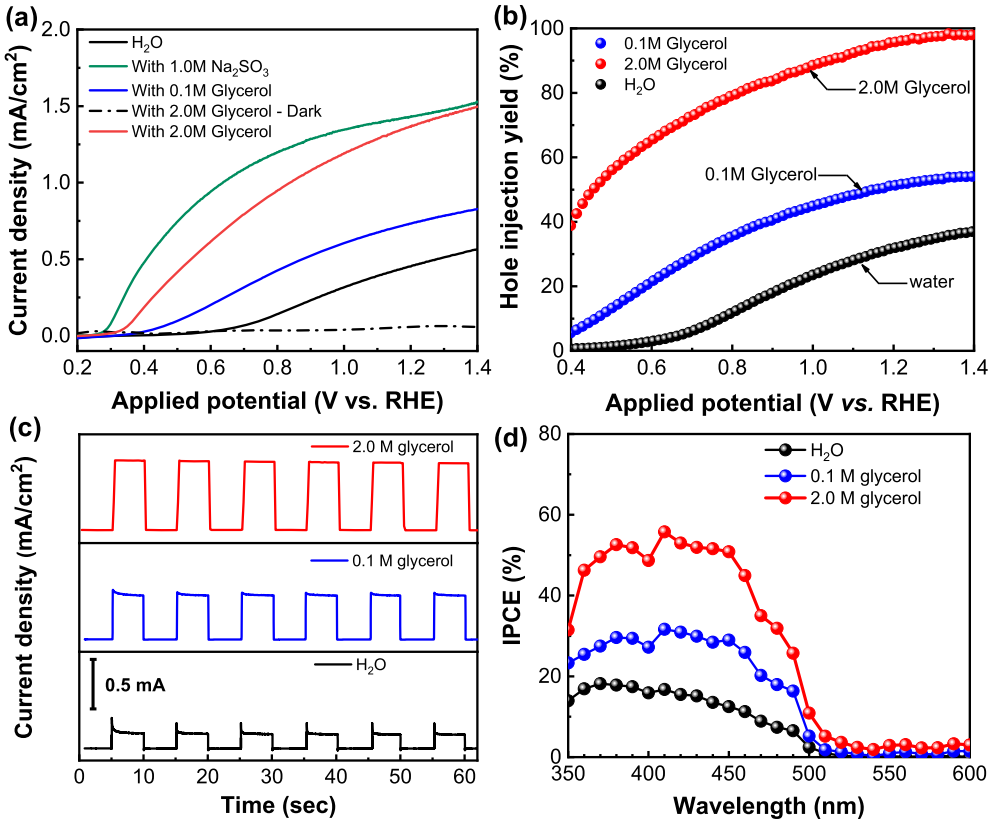

Fig. 5. (a) Current (J)-potential (V) curves and (b) their corresponding hole injection efficiency for water, glycerol and sulfide oxidations; (c) photocurrent vs. time measurements performed with chopped light at 0.7 V vs. RHE and (d) external quantum efficiency (IPCE) of $BiVO_4$ photoanode measured at 1.23 V vs. RHE with various glycerol concentrations.

$$J_{ph}^{sulfite} = J_{abs} \times \eta_{sep} \times 100\% \quad (4)$$

$$\eta_{inj} = \frac{J_{ph}^{rxn}}{J_{ph}^{sulfite}} \quad (5)$$

As in Fig. 5(b), for both glycerol and glycerol oxidation, at a higher applied potential, a higher hole injection efficiency was observed. The water oxidation by $BiVO_4$ photoanode showed that ~32% of the hole reaching the electrode surface can be injected into the electrolyte for water oxidation reaction at 1.23 V vs. RHE. However, the injection efficiency increased to ~52% and ~96% for the 0.1 M and 2 M glycerol oxidation reaction, respectively. This indeed demonstrated that the high kinetics towards glycerol oxidation reaction on the $BiVO_4$ photoanode. Thus, adding glycerol into the electrolyte can highly increase the PEC efficiency by boosting the hole injection efficiency. Furthermore, Fig. 5(c) shows the result of transient photocurrent measurement of $BiVO_4$ photoanode with the addition of glycerol into the electrolyte. As shown in the figure, in absence of glycerol, the transient spikes were much sharper than those of with glycerol, indicating the fast recombination of photogenerated pairs of electron-hole for the water oxidation reaction. Conversely, with the presence of 0.1 M glycerol in the electrolyte, the recombination was significant suppressed and the decay of currents to the steady-state values took longer time. More interestingly, when 2 M glycerol was added, the square transient photocurrent response was observed, revealing that the recombination was completely suppressed. In other words, the consumption of holes from the photoanode in presence of glycerol was much more efficient and it was again due to the high kinetics towards glycerol oxidation. Additionally, external quantum yields (i.e. IPCE) of $BiVO_4$ photoanodes in the wavelength range of 350–550 nm, which were acquired at $1.23V_{RHE}$, were also measured and shown in Fig. 5(d). Apparently, adding glycerol can enhance the IPCE significantly in comparison with that of water oxidation reaction only. The IPCE value of $BiVO_4$ photoanode for 2 M glycerol reached about 55% in the range from 350 to 450 nm, which was nearly 3 times higher than that of OER system. Given that adding glycerol would not significantly alter the photoanode light absorption profile, the higher IPCE value of $BiVO_4$ in presence of glycerol revealed that the photoexcited holes successfully transferred and participated in photoelectrochemical reaction with much less efficiency loss [37].

3.3. Product analysis and proposed mechanism

It would not be practical to run a large-scale energy conversion system at high applied bias because the energy input required to sustain the bias would compromise the energy output. Therefore, in this study, the continuous oxidation of glycerol was studied at 0.7 V_{RHE} which was high enough to oxidize glycerol efficiently without OER occurring. The corresponding current density and reaction products were shown in Fig. S2 and Fig. 6. As revealed in Fig. S2 and S3, despite the $BiVO_4$ photoanode suffered some deterioration initially but then the current density maintained constant for at least 7 h, suggesting a reasonable stability for the PEC glycerol oxidation which was consistent with structure and chemical state analysis shown in Fig. S4. Additionally, ICP was also performed to further investigate the dissolution of $BiVO_4$. As shown in Table S1, fresh and post glycerol oxidation electrolyte both had similar Bi and V amount while $BiVO_4$ film was kept the ratio of Bi:V = 1:1.

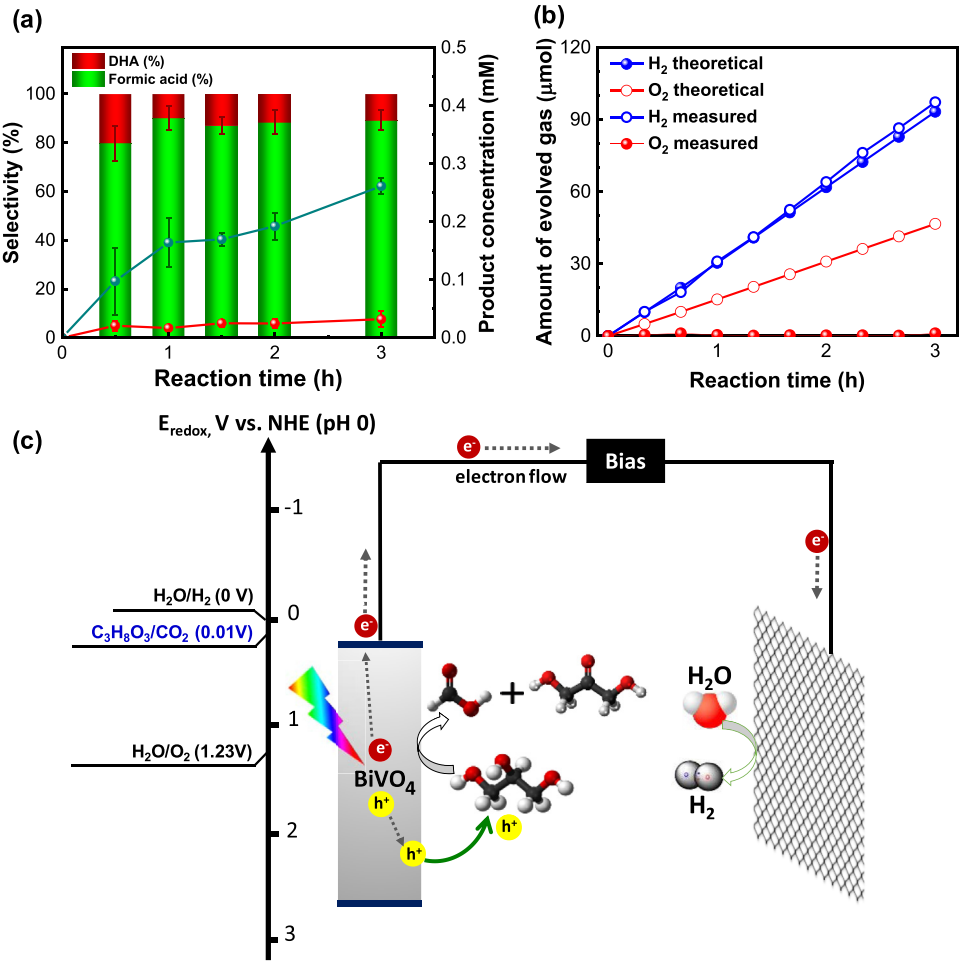

Fig. 6. (a) Plot giving the concentration and selectivity of liquid products vs. time; (b) Gaseous products obtained during the glycerol electrooxidation on $BiVO_4$ photoanode at 0.7 V vs. RHE; (c) Schematic representation of the energy band diagram of the $BiVO_4$ photoanode in contact with solution during PEC glycerol oxidation.

Therefore, it is reasonably to believe that there was no significant dissolution of the $BiVO_4$ during the glycerol oxidation. It is interesting to note that, the durability of $BiVO_4$ in glycerol oxidation was more stable than that of water oxidation only (Fig. S5). It has been previously reported that if the consumption of the surface-reaching holes for the interfacial oxidation reaction is fast enough so that no holes accumulating on the surface, much better stability could be achieved [38]. To further understand the oxidation of glycerol on the $BiVO_4$ photoanode, the liquid products of glycerol oxidation for 3 h under continuously illumination on $BiVO_4$ photoanode was analyzed by HPLC (Fig. 6(a)). The products were identified as formic acid and dihydroxyacetone (DHA) with the selectivity of ~85% for formic acid ~15% for DHA, respectively. Moreover, the theoretical production of each products was given in Fig. S6 with the assumption of all the current was contributed into one product at a time. It is worth to note that DHA is used as an active ingredient in the sunless tanners with very high value (ca. 150 USD/kg) in comparison to the price of both crude and purified glycerol (<0.3 USD/kg and ~0.6 USD/kg, respectively) [39]. The selectivity of DHA by our $BiVO_4$ photoanode was much higher than those selectivity (4–7%) obtained from TiO_2 [15,16]. Even more, it was surprisingly higher than some of the precious metal-containing carbon-based materials, like carbon nanotube, carbon nanofiber and reduced graphene oxide, whose selectivity towards DHA were around 5–9% [18,21,22]. Furthermore, besides from DHA, there is no doubt about the importance of the formic acid (~110 USD/kg for 95%) in the various chemical industries. Additionally, the gas evolution collected from the air-tight PEC cell further confirmed that the theoretical and measured hydrogen gas from water splitting was matched and there was no detectable oxygen due to the water oxidation reaction was taken over by the glycerol oxidation. Based on the above discussion, the proposed mechanism for solar-driven glycerol oxidation over $BiVO_4$ photoanode was proposed and illustrated in Fig. 6(c). Under light irradiation, the holes (h^+) generated from $BiVO_4$ migrated into electrode/electrolyte interface and reacted with glycerol. The DHA was formed by the secondary -OH oxidation and the formic acid was resulted from the further oxidation process involving the C-C cleavage. Meanwhile, the photogenerated electrons (e^-) migrated to counter electrode (Pt) for hydrogen evolution reaction. Therefore, it is reasonable to conclude that the photoelectrochemical water splitting in glycerol aqueous solution not only boost the hydrogen evolution rate but also enhance the photoelectrochemical stability of $BiVO_4$ electrode as well as add the extra value to the biodiesel plant.

4. Conclusions

In summary, we introduced a high-performance photoelectrochemical cell based on bismuth vanadate by introducing the industrial by-product, i.e. glycerol. With adding glycerol at an appropriate concentration, surface charge recombination in bismuth vanadate photoanode is near-completely suppressed and

thus PEC performance is vastly enhanced. Additionally, the presence of glycerol can greatly reduce the requirement of larger anodic potentials for PEC hydrogen evolution and facilitate the production of valuable organic compounds. This work not only provides a simple and cost-effective approach to boost the hydrogen production efficiency but also to make the biodiesel production more profitable and sustainable.

Acknowledgments

This work was financially supported from the Young Scholar Fellowship Program by Ministry of Science and Technology (MOST) in Taiwan, under Grant MOST108-2636-E-011-001. The authors would like to express their gratitude to National Taiwan University of Science and Technology for facilities support.

Appendix A. Supplementary data

Supplementary data to this article can be found online at https://doi.org/10.1016/j.electacta.2019.134725.

References

[1] H.J. Kim, Y. Kim, D. Lee, J.-R. Kim, H.-J. Chae, S.-Y. Jeong, B.-S. Kim, J. Lee, G.W. Huber, J. Byun, S. Kim, J. Han, Coproducing value-added chemicals and hydrogen with electrocatalytic glycerol oxidation Technology: experimental and techno-economic investigations, ACS Sustain. Chem. Eng. 5 (2017) 6626–6634.
[2] M.A. Dasari, P.-P. Kiatsimkul, W.R. Sutterlin, G.J. Suppes, Low-pressure hydrogenolysis of glycerol to propylene glycol, Appl. Catal. Gen. 281 (2005) 225–231.
[3] J.-M. Clacens, Y. Pouilloux, J. Barrault, Selective etherification of glycerol to polyglycerols over impregnated basic MCM-41 type mesoporous catalysts, Appl. Catal. Gen. 227 (2002) 181–190.
[4] C.-Y. Chiang, Y.-S. Chen, M.-S. Liang, F.-Y. Lin, C.Y.-D. Tai, H.-S. Liu, Absorption of ethanol into water and glycerol/water solution in a rotating packed bed, J. Taiwan Inst. Chem. Eng. 40 (2009) 418–423.
[5] C.-Y. Chiang, D.-W. Lee, H.-S. Liu, Carbon dioxide capture by sodium hydroxide-glycerol aqueous solution in a rotating packed bed, J. Taiwan Inst. Chem. Eng. 72 (2017) 29–36.
[6] Z. Zhang, L. Xin, J. Qi, D.J. Chadderdon, K. Sun, K.M. Warsko, W. Li, Selective electro-oxidation of glycerol to tartronate or mesoxalate on Au nanoparticle catalyst via electrode potential tuning in anion-exchange membrane electrocatalytic flow reactor, Appl. Catal. B Environ. 147 (2014) 871–878.
[7] C.H. Lam, A.J. Bloomfield, P.T. Anastas, A switchable route to valuable commodity chemicals from glycerol via electrocatalytic oxidation with an earth abundant metal oxidation catalyst, Green Chem. 19 (2017) 1958–1968.
[8] C. Len, R. Luque, Continuous flow transformations of glycerol to valuable products: an overview, Sustain. Chem. Process. 2 (2014) 1.
[9] S. Ardo, D. Fernandez Rivas, M.A. Modestino, V. Schulze Greiving, F.F. Abdi, E. Alarcon Llado, V. Artero, K. Ayers, C. Battaglia, J.-P. Becker, D. Bederak, A. Berger, F. Buda, E. Chinello, B. Dam, V. Di Palma, T. Edvinsson, K. Fujii, H. Gardeniers, H. Geerlings, S.M.H. Hashemi, S. Haussener, F. Houle, J. Huskens, B.D. James, K. Konrad, A. Kudo, P.P. Kunturu, D. Lohse, B. Mei, E.L. Miller, G.F. Moore, J. Muller, K.L. Orchard, T.E. Rosser, F.H. Saadi, J.-W. Schüttauf, B. Seger, S.W. Sheehan, W.A. Smith, J. Spurgeon, M.H. Tang, R. van de Krol, P.C.K. Vesborg, P. Westerik, Pathways to electrochemical solar-hydrogen technologies, Energy Environ. Sci. 11 (2018) 2768–2783.
[10] C. Palmer, F. Saadi, E.W. McFarland, Technoeconomics of commodity chemical production using sunlight, ACS Sustain. Chem. Eng. 6 (2018) 7003–7009.
[11] B. Mei, G. Mul, B. Seger, Beyond water splitting: efficiencies of photoelectrochemical devices producing hydrogen and valuable oxidation products, Adv. Sustain. Syst. 1 (2017) 1600035.
[12] S. Hu, Membrane-less photoelectrochemical devices for H2O2 production: efficiency limit and operational constraint, Sustain. Energy Fuels 3 (2019) 101–114.
[13] B. Zhang, J. Shi, C. Ding, R. Chong, B. Zhang, Z. Wang, A. Li, Z. Liang, S. Liao, C. Li, Conversion of biomass derivatives to electricity in photo fuel cells using undoped and tungsten-doped bismuth vanadate photoanodes, ChemSusChem 8 (2015) 4049–4055.
[14] A. Fujishima, K. Honda, Electrochemical photolysis of water at a semiconductor electrode, Nature 238 (1972) 37–38.
[15] V. Augugliaro, H.A.H. El Nazer, V. Loddo, A. Mele, G. Palmisano, L. Palmisano, S. Yurdakal, Partial photocatalytic oxidation of glycerol in TiO2 water suspensions, Catal. Today 151 (2010) 21–28.
[16] J. Han, Y. Kim, H.W. Kim, D.H.K. Jackson, D. Lee, H. Chang, H.-J. Chae, K.-Y. Lee, H.J. Kim, Effect of atomic-layer-deposited TiO2 on carbon-supported Ni catalysts for electrocatalytic glycerol oxidation in alkaline media, Electrochem. Commun. 83 (2017) 46–50.
[17] L. Guo, Q. Sun, K. Marcus, Y. Hao, J. Deng, K. Bi, Y. Yang, Photocatalytic glycerol oxidation on AuxCu–CuS@TiO2 plasmonic heterostructures, J. Mater. Chem. 6 (2018) 22005–22012.
[18] L.S. Ribeiro, E.G. Rodrigues, J.J. Delgado, X. Chen, M.F.R. Pereira, J.J.M. Órfão, Pd, Pt, and Pt–Cu catalysts supported on carbon nanotube (CNT) for the selective oxidation of glycerol in alkaline and base-free conditions, Ind. Eng. Chem. Res. 55 (2016) 8548–8556.
[19] E.G. Rodrigues, M.F.R. Pereira, X. Chen, J.J. Delgado, J.J.M. Órfão, Selective oxidation of glycerol over platinum-based catalysts supported on carbon nanotubes, Ind. Eng. Chem. Res. 52 (2013) 17390–17398.
[20] S. Demirel, K. Lehnert, M. Lucas, P. Claus, Use of renewables for the production of chemicals: glycerol oxidation over carbon supported gold catalysts, Appl. Catal. B Environ. 70 (2007) 637–643.
[21] M. Zhang, R. Nie, L. Wang, J. Shi, W. Du, Z. Hou, Selective oxidation of glycerol over carbon nanofibers supported Pt catalysts in a base-free aqueous solution, Catal. Commun. 59 (2015) 5–9.
[22] M. Zhang, J. Shi, W. Ning, Z. Hou, Reduced graphene oxide decorated with PtCo bimetallic nanoparticles: facile fabrication and application for base-free oxidation of glycerol, Catal. Today 298 (2017) 234–240.
[23] Y. Kwon, Y. Birdja, I. Spanos, P. Rodriguez, M.T.M. Koper, Highly selective electro-oxidation of glycerol to dihydroxyacetone on platinum in the presence of bismuth, ACS Catal. 2 (2012) 759–764.
[24] S. Lee, H.J. Kim, E.J. Lim, Y. Kim, Y. Noh, G.W. Huber, W.B. Kim, Highly selective transformation of glycerol to dihydroxyacetone without using oxidants by a PtSb/C-catalyzed electrooxidation process, Green Chem. 18 (2016) 2877–2887.
[25] T.-G. Vo, J.-M. Chiu, C.-Y. Chiang, Y. Tai, Solvent-engineering assisted synthesis and characterization of $BiVO_4$ photoanode for boosting the efficiency of photoelectrochemical water splitting, Sol. Energy Mater. Sol. Cells 166 (2017) 212–221.
[26] B.E. Wu, C.Y. Chiang, Photochemical metal organic deposition of FeO_x catalyst on $BiVO_4$ for improving solar-driven water oxidation efficiency, J. Taiwan Inst. Chem. Eng. 80 (2017) 1014–1021.
[27] L. Zhang, E. Reisner, J.J. Baumberg, Al-doped ZnO inverse opal networks as efficient electron collectors in $BiVO_4$ photoanodes for solar water oxidation, Energy Environ. Sci. 7 (2014) 1402.
[28] T.-G. Vo, J.-M. Chiu, Y. Tai, C.-Y. Chiang, Turnip-inspired $BiVO_4$/CuSCN nanostructure with close to 100% suppression of surface recombination for solar water splitting, Sol. Energy Mater. Sol. Cells 185 (2018) 415–424.
[29] J.A. Seabold, K. Zhu, N.R. Neale, Efficient solar photoelectrolysis by nanoporous Mo:$BiVO_4$ through controlled electron transport, Phys. Chem. Chem. Phys. 16 (2014) 1121–1131.
[30] D.K. Zhong, S. Choi, D.R. Gamelin, Near-complete suppression of surface recombination in solar photoelectrolysis by “Co-Pi” catalyst-modified W:BiVO4, J. Am. Chem. Soc. 133 (2011) 18370–18377.
[31] F.F. Abdi, R. van de Krol, Nature and light dependence of bulk recombination in Co-Pi-Catalyzed $BiVO_4$ photoanodes, J. Phys. Chem. C 116 (2012) 9398–9404.
[32] C.A. Mesa, A. Kafizas, L. Francàs, S.R. Pendlebury, E. Pastor, Y. Ma, F. Le Formal, M.T. Mayer, M. Grätzel, J.R. Durrant, Kinetics of photoelectrochemical oxidation of methanol on hematite photoanodes, J. Am. Chem. Soc. 139 (2017) 11537–11543.
[33] M. Ibadurrohman, K. Hellgardt, Photoelectrochemical performance of graphene-modified TiO2 photoanodes in the presence of glycerol as a hole scavenger, Int. J. Hydrogen Energy 39 (2014) 18204–18215.
[34] X. Lu, S. Xie, H. Yang, Y. Tong, H. Ji, Photoelectrochemical hydrogen production from biomass derivatives and water, Chem. Soc. Rev. 43 (2014) 7581–7593.
[35] S.K. Mohapatra, K.S. Raja, V.K. Mahajan, M. Misra, Efficient photoelectrolysis of water using TiO2 nanotube Arrays by minimizing recombination losses with organic additives, J. Phys. Chem. C 112 (2008) 11007–11012.
[36] T.G. Vo, Y. Tai, C.Y. Chiang, Multifunctional ternary hydrotalcite-like nanosheet arrays as an efficient co-catalyst for vastly improved water splitting performance on bismuth vanadate photoanode, J. Catal. 370 (2019) 1–10.
[37] T.W. Kim, K.-S. Choi, Nanoporous $BiVO_4$ photoanodes with dual-layer oxygen evolution catalysts for solar water splitting, Science 343 (2014) 990–994, 80-.
[38] D.K. Lee, K.-S. Choi, Enhancing long-term photostability of $BiVO_4$ photoanodes for solar water splitting by tuning electrolyte composition, Nat. Energy. 3 (2017) 53–60.
[39] B. Katryniok, H. Kimura, E. Skrzyńska, J.-S. Girardon, P. Fongarland, M. Capron, R. Ducoulombier, N. Mimura, S. Paul, F. Dumeignil, Selective catalytic oxidation of glycerol: perspectives for high value chemicals, Green Chem. 13 (2011) 1960–1979.